AIAA JOURNAL
Vol. 49, No. 11, November 2011

Modification of Transonic Blowdown Wind Tunnel to Produce Oscillating Freestream Mach Number

Kyle Gompertz, Christopher Jensen, Pradeep Kumar, Di Peng, James W. Gregory, and Jeffrey P. Bons
Ohio State University, Columbus, Ohio 43235

DOI: 10.2514/1.J051090

This paper details the design, construction, and evaluation of a modification to Ohio State University's 6 × 22 in. transonic wind tunnel to enable modulation of the freestream Mach number. The test-section Mach number in this blowdown facility is dynamically set by varying the choke area in a harmonic fashion. Disturbances from the modulated throat area propagate upstream to vary the test-section Mach number. Flow properties, such as wave propagation speed, were evaluated using one-dimensional theory, two-dimensional computational fluid dynamics, and experiments in order to understand the fundamental mechanisms of the Mach number oscillation process and subsequent performance limitations of the facility. The current configuration of the facility can produce Mach number oscillations between 0.44 and 0.65 for a Reynolds number range of 17–43 million per meter at sufficiently low oscillation frequencies. The control frequency can be varied up to 25 Hz, although the wind tunnel emulates a low-pass filter with a −3 dB cutoff frequency of approximately 8 Hz.

Nomenclature

A	=	test-section area, m^2
a	=	sonic velocity, m/s
A^*	=	choke area, m^2
B	=	amplitude of backpressure oscillation, kPa
c	=	upstream propagating wave speed, m/s
d	=	major axis of choke vane profile, cm
d_w	=	hot-film diameter, μm
E	=	hot-film Wheatstone bridge voltage, V
e	=	minor axis of choke vane profile, cm
F	=	hot-film calibration coefficient
f	=	oscillation frequency, Hz
G	=	hot-film calibration coefficient
H	=	tunnel height at choke vane location, cm
L	=	distance from throat to stagnation chamber, m
k	=	thermal conductivity of air, W/m · K
M	=	Mach number
m	=	wave number
Nu	=	Nusselt number
n	=	hot-film calibration equation exponent
P	=	pressure, Pa
p	=	temperature correction exponent
Pr	=	Prandtl number
R	=	resistance, Ω
r	=	radius of wind-tunnel stagnation chamber, m
Re	=	Reynolds number
T	=	temperature, K
t	=	time, s
V	=	tunnel stagnation chamber volume, m^3
x	=	streamwise direction, m
γ	=	ratio of specific heats
θ	=	angular position, rad
φ	=	phase shift, rad
ω	=	oscillation frequency, rad/s

Subscripts

avg	=	average conditions
CV	=	choke vane rotation
exit	=	tunnel exit conditions
f	=	flow conditions
M	=	Mach number oscillation frequency
S	=	static conditions
STP	=	standard atmosphere conditions
T	=	stagnation conditions
w	=	hot-film operating conditions

Presented as Paper 2010-1484 at the 48th AIAA Aerospace Sciences Meeting Including the New Horizons Forum and Aerospace Exposition, Orlando, FL, 4–7 January 2010; received 22 November 2010; revision received 26 January 2011; accepted for publication 1 February 2011.

I. Introduction

UNSTEADY wind tunnels are relatively uncommon, but they are important tools for investigation of unsteady aerodynamic phenomena. Flow phenomena such as dynamic stall, flutter, and gust response all require appropriate experimental modeling in order to fully investigate the flow details. Many unsteady testing situations involve the dynamic movement of a model in the wind-tunnel test section. These methods provide suitable simulation of moving bodies in a fluid; however, the effects due to varying flow conditions are not adequately modeled by model movement alone due to viscous and compressibility effects. Flow situations such as gust response or a rotor blade in forward flight require a wind tunnel where the test-section velocity can be oscillated at an appropriate physical frequency. There are very few wind tunnels in existence that can achieve oscillatory flow. The Klebanoff–Saric Unsteady Wind Tunnel, recently reconstructed at Texas A&M University, is a low-turbulence tunnel capable of 36 m/s flow and oscillation frequencies up to 25 Hz [1]. Its high flow quality has made it suitable for extensive fundamental investigations into laminar-turbulent transition mechanisms. Retelle et al. [2] reported the development of a 16 m/s wind tunnel with 2 Hz oscillations at the University of Colorado. Pierce et al. [3] developed a modification to the Georgia Institute of Technology low-turbulence wind tunnel, where flows of up to 21 m/s could be modulated at rates up to 2 Hz. The development of a low-speed wind tunnel at the Institut de Méchanique des Fluides de Marseille was reported by Favier et al. [4–6] and Maresca et al. [7]. This facility employs a two-degree-of-freedom moving mounting rig that oscillates an airfoil in pitch and translation at rates up to 5 Hz in 25 m/s flow. Ham et al. [8] describe how airflow through the Wright Brothers Wind Tunnel at the Massachusetts Institute of Technology is modulated to simulate rotorcraft airfoil response to lateral and longitudinal gusts. Modulation up to 1.5 times per rotor revolution in

$M < 0.2$ flow is accomplished using slotted blowing to vary the circulation about twin airfoils mounted upstream of the rotor plane. Szumowski and Meier [9] and Selerowicz and Szumowski [10] discuss a transonic wind tunnel with perturbations over a range of 55 to 116 Hz at a Mach number of 0.7, although it is not clear that the flow throughout the test section was modulated. Babinsky and Fernie [11–14] and Bruce and Babinsky [15] converted a transonic/supersonic blowdown wind-tunnel facility for unsteady freestream oscillations by installing a rotating cam obstruction downstream of the test section. Their wind tunnel can operate up through supersonic conditions [15] with freestream oscillation frequencies ranging from 5 to 180 Hz [11]. All of these example facilities allow for oscillation of the tunnel freestream velocity, but most are strictly limited to the incompressible flow regime ($M < 0.1$). There is a significant lack of facility capability for freestream modulation of compressible flows.

This work is motivated by the need for a transonic wind tunnel that can produce dynamically varying Mach number for complete simulation of compressible unsteady flow phenomena. The 6×22 in. transonic wind tunnel in the Aeronautical and Astronautical Research Laboratory (AARL) at Ohio State University (OSU) has been modified to enable dynamic test-section Mach number oscillations. The work presented in this paper involves the implementation of one-dimensional (1-D) theory, unsteady two-dimensional (2-D) computational fluid dynamics (CFD) simulations, and experimental measurement to elucidate the fundamental mechanisms that produce the oscillations in freestream Mach number. These investigative techniques were used to characterize the flow situation and establish limitations on facility performance.

II. Experimental Facility

A. Six by 22-Inch Transonic Wind Tunnel

OSU's transonic wind tunnel was designed specifically for the testing of airfoils. Starting in 1976, the 6×22 in. transonic wind tunnel was used as the key experimental facility for the General Aviation Airfoil Design and Analysis Service. During this period of time, a plethora of airfoils were tested and developed at OSU for the aeronautical community [16,17].

A layout of the tunnel can be seen in Fig. 1. The wind tunnel was designed as a low-turbulence facility, with the primary goal of matching freestream flight conditions. To accomplish this, the settling chamber is equipped with a perforated plate, honeycomb section, and then eight screens (60 mesh) lower the turbulence to acceptable levels (less than 0.5%) under steady flow conditions. A subsonic nozzle with a contraction ratio of 15:1 provides excellent flow uniformity in the 6×22 in. test section, which is 1.1 m long. The 56-cm-high (22-in.-high) solid sidewalls hold the airfoil. The 15 cm (6 in.) spanwise floor and ceiling walls are perforated with 3.2 mm straight holes yielding an effective porosity of 6% [18]. These isolation cavities or plenums are open to the flow only downstream of the test section and aid in producing a high-quality flow in the test section by reducing Mach wave reflections in transonic flow. The tunnel is fed by two 21 m^3 tanks pressurized up to 15.5 MPa, with conventional air dryers used to maintain gas purity. The high-pressure air is controlled by two valves. The first is a control valve that sets the total pressure and Reynolds number. The second valve is a fast-acting valve used to start and stop the flow. The Mach number is controlled independently of the Reynolds number by adjusting the throat area downstream of the test section. The Mach number is uniquely set by the throat area, independent of stagnation pressure, as long as choked flow is maintained. The two parameters (Re and M) can be independently varied over a considerable range, as shown in Fig. 2.

B. Freestream Oscillation Device

In the current configuration, the transonic tunnel has been modified to allow freestream velocity modulation up to 25 Hz using a variable-area throat downstream of the test section. In the conventional time-invariant configuration, the Mach number is set by the cross-sectional area A^* at a choke point downstream of the test section, as shown in Fig. 1. Since the blowdown tunnel is choked at the throat, the test-section Mach number is uniquely set by the area ratio, independent of the stagnation pressure according to the area-Mach number relation expressed in Eq. (1) for steady, inviscid 1-D flow:

$$\frac{A}{A^*} = \frac{1}{M}\left[\left(\frac{2}{\gamma+1}\right)\left(1+\frac{\gamma-1}{2}M^2\right)\right]^{(\gamma+1)/[2(\gamma-1)]} \tag{1}$$

Thus, the Mach number of the flow is set independently of the Reynolds number. The modification uses rotating elongated vanes to control the throat cross-sectional area as a function of time. A drive mechanism rotates four vanes, as shown in Fig. 3. Figure 3a is an isometric view of the hardware employed to operate the choke vanes, and Fig. 3b is a view of the choke vane installation as seen looking upstream from the tunnel exit. The vane assembly is driven by a 5 hp

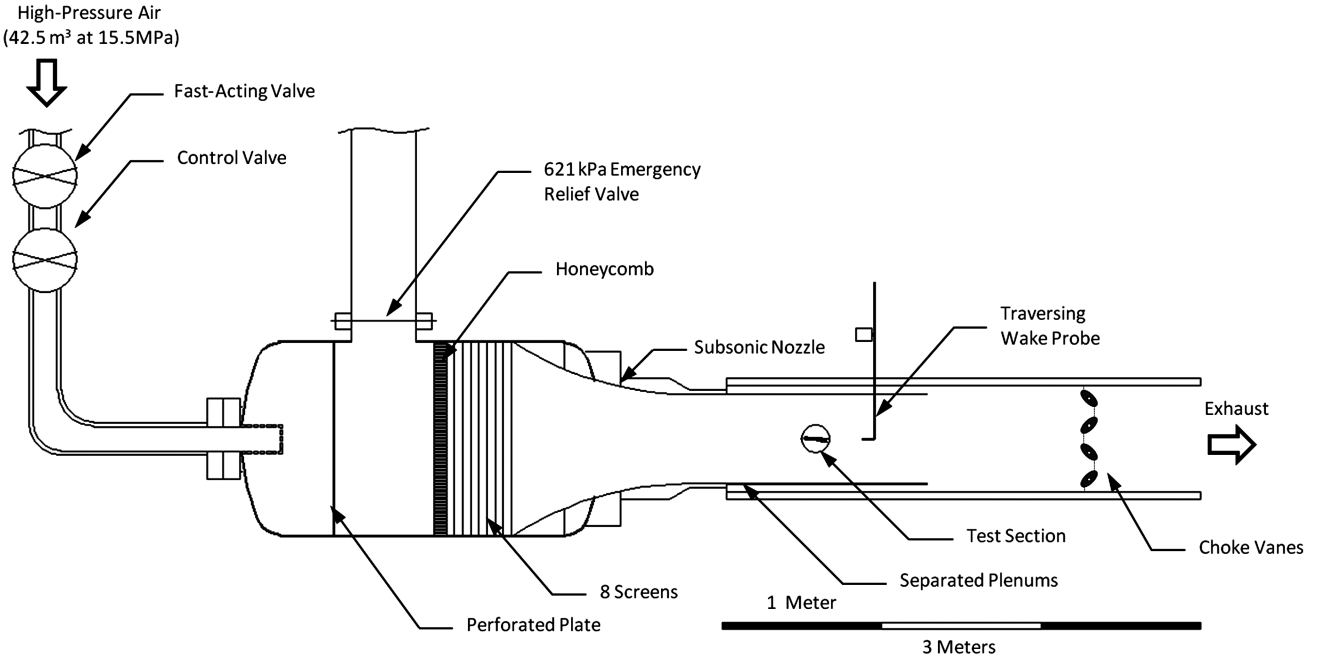

Fig. 1 Schematic of the AARL 6 × 22 in. (15 × 56 cm) transonic wind tunnel.

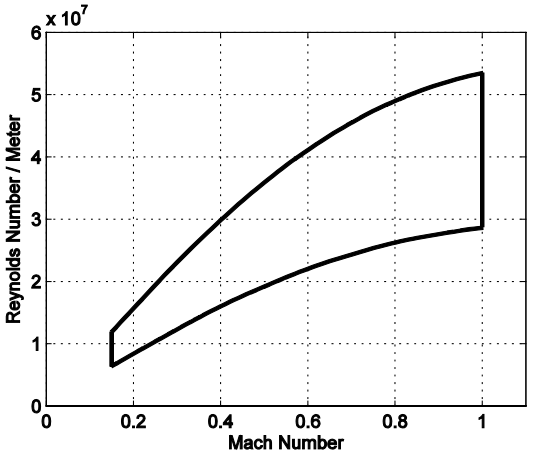

Fig. 2 Range of test-section operating conditions for the 6 × 22 in. transonic wind tunnel at 280 K and a maximum operating pressure of 345 kPa.

variable-frequency ac motor. The drive chain is coupled to a flywheel and configured such that adjacent vanes are counter rotating to minimize the unsteady aerodynamic loads on the transmission. The vane profile is displayed in Fig. 4. As the vanes rotate, the open cross-sectional area is varied between maximum and minimum values, as illustrated by the time history of A^* inset in Fig. 4. The cross-sectional area of the vanes was specified such that the vane rotation produces a near-sinusoidal Mach number oscillation in the test section. The amplitude of Mach number oscillation is set by the dimensions of the major d and minor e axes of the rotating vanes. The geometrical configuration of the oscillating vanes may be adjusted between runs in a relatively short period of time by interchanging between several sets of prefabricated vane assemblies to produce varied Mach number waveforms.

A shaft-mount optical encoder was coupled to the shaft of the uppermost sprocket to index each full revolution (1/rev) and the angular orientation of the choke vanes (500/rev). The signal was used to determine the oscillation frequency, the instantaneous angular position θ_{CV}, the angular rate of rotation ($d\theta_{CV}/dt$), and the phase delay φ between the choke vane position and the unsteady test-section Mach number.

C. Instrumentation

The wind tunnel is equipped with 11 pressure taps of 0.8 mm diameter along the sidewalls at midheight, as shown along with other equipment in Fig. 5. These taps were selectively connected to a pair of 350 kPa high-speed absolute pressure transducers to obtain static pressure data along the streamwise x direction. The transducers have a calibration uncertainty of ±690 Pa and a frequency response

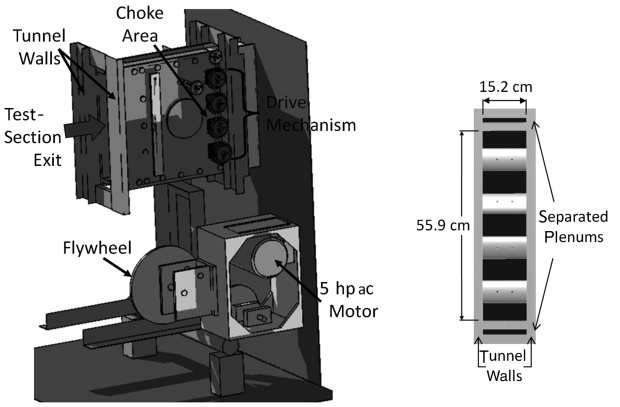

a) Mach number oscillation mechanism **b) Aft-looking upstream at vane installation**

Fig. 3 Schematic of tunnel modification hardware.

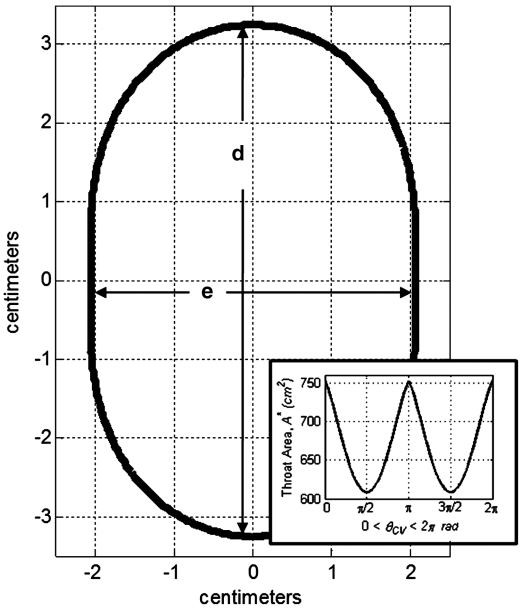

Fig. 4 Geometric choke vane profile constructed to produce approximately sinusoidal Mach number oscillation. Choke vane profile plotted for $\theta_{CV} = \pi/2 + m\pi$. The inset shows the throat area A^* as a function of choke vane angular position.

greater than 300 Hz. Tests were conducted to determine the speed at which the oscillating disturbance propagates upstream from the throat to the test section (tap 3). For these surveys, one pressure transducer was wall-mounted and fixed at the test-section location, while the other transducer was wall-mounted at various positions along the length of the tunnel for each run. A temporal correlation was performed between the pressure signals to determine the phase lag in the disturbance between any two pressure tap locations. Sampling the pressure signals at 10 kHz, the systematic uncertainty in the measured time shift Δt is ±0.05 ms [19].

Additionally, a pitot probe with a 0.8 mm sensing orifice was used to measure the stagnation pressure near the midheight at a position 0.3 m downstream of the test-section static pressure tap (refer to Fig. 5). Thus, the test-section Mach number can be calculated from pressure data, assuming isentropic quasi-steady flow conditions. However, the measured frequency response of this instrument is approximately 15 Hz, which is inadequate for characterizing the unsteady flow in the modified wind tunnel. Consequently, data acquired with the pitot probe are primarily used to perform an in situ calibration of a hot-film probe while the Mach number oscillation frequency is nominally 2 Hz.

Measurements were made of the magnitude and phase relationships of the oscillating airstream throughout the wind tunnel at unsteady Mach numbers ranging between $0.44 < M < 0.65$ and at various Mach number oscillation frequencies f_M up to 25 Hz. The oscillations of the airstream in the test section were measured by a hot-film mounted on the surface of a conical probe (TSI model 1231-60W) aligned with the freestream. A thin platinum film strip of 7.6 μm diameter (d_w) is wrapped around the conical probe tip. The hot-film signal was sampled at 10 kHz and low-pass filtered at 5 kHz to attenuate noise.

An in situ calibration technique was developed to cope with the low frequency response of the pitot probe and observed run-to-run variations of the hot-film heat transfer characteristics and flow temperature T_f. The pressure and hot-film signals acquired during each test were saved on a hard disk, and the film calibration was performed as a postprocessing step. All hot-film data have been reduced based on the in situ calibration, which was achieved by rotating the choke vanes at low frequencies for an interval at the beginning and end of each run to span a range of flow temperature. A type K thermocouple located in the stagnation tank was used to measure the stagnation temperature and calculate the sonic velocity. During a 30 s run, T_f typically decreases 15 K, corresponding to a

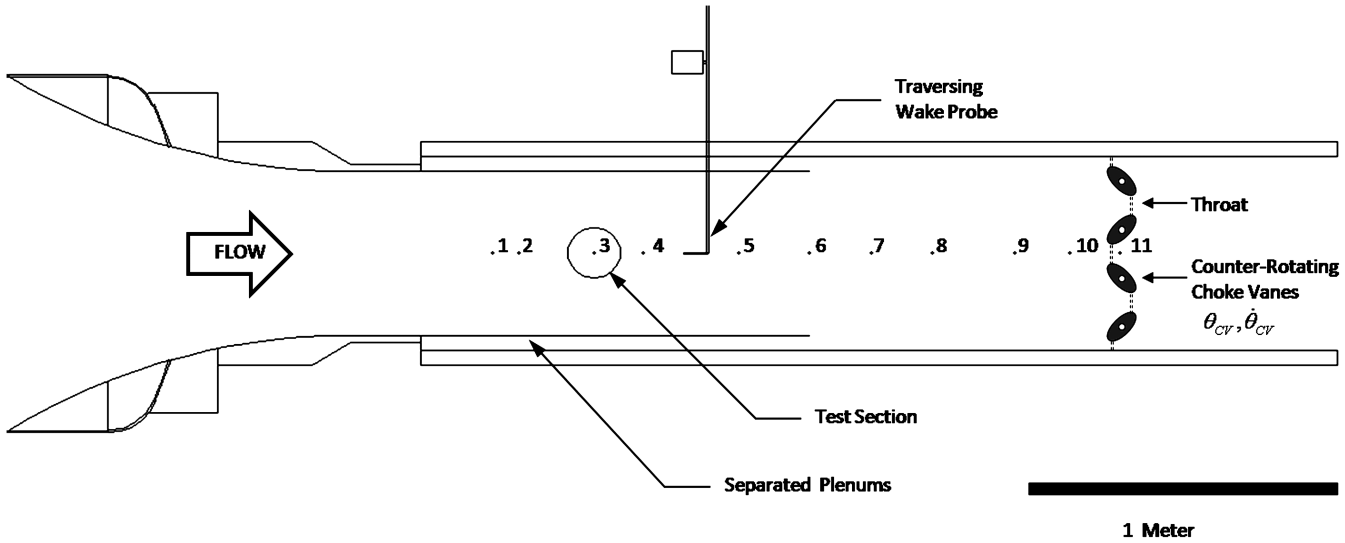

Fig. 5 Schematic of the AARL 6 × 22 in. transonic wind tunnel, shown in a configuration that produces an oscillating Mach number in the test section. Note that the static pressure taps are numbered 1–11. The hot film is colocated with tap 3.

7.5 m/s decrease in the speed of sound a. Thus, the expression for the nondimensional heat transfer coefficient, Nu_{STP} in Eq. (2), can be corrected for temperature variation as described by Collis and Williams [20]. This is accomplished iteratively by solving for the temperature-ratio exponent p such that the calibration oscillations collapse on the best-fit calibration curve given by Eq. (3), where F, G, and n are calibration coefficients. An example Mach number time history is displayed in Fig. 6. The oscillation frequency of 2 Hz was sufficiently low to be accurately resolved with the pressure transducers without dynamic response issues. Mach number data were obtained via a colocated static pressure tap (in the test section) and a pitot probe positioned 0.3 m downstream of the hot film. A temporal correlation analysis was performed to correct for the pitot tube length and the phase lag between the stagnation and static pressure measurement locations. In the current configuration, the time correction was approximately 30 ms. A correction was also applied to align the calculated velocity (from the pressure data) in time with the hot-film signal (6 ms shift). The test-section velocity measured by the hot film is obtained from the Reynolds number, which is correlated directly to the Nu_{STP}. For the Mach number expressed as a function of pressure, flow temperature, and hot-film bridge voltage, the uncertainty in the measured Mach number is ±0.005 at a nominal Mach number of 0.51:

$$Nu_{\mathrm{STP}} = \frac{E^2 \cdot (T_{\mathrm{avg}}/T_f)^p [R_w/(R_w + 10)^2] \cdot Pr^{-1/3}}{k\pi d_w (T_w - T_f)} \tag{2}$$

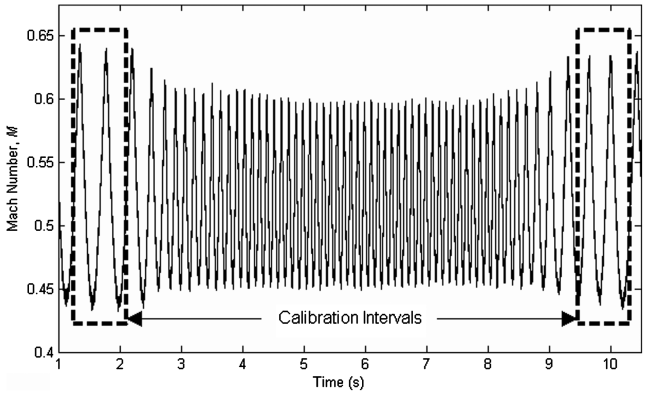

Fig. 6 Representative oscillating Mach number measurements made with the hot-film anemometer.

$$Nu_{\mathrm{STP}} = F + G \cdot Re^n \tag{3}$$

Knowledge of freestream turbulence information may be necessary to properly interpret data acquired about airfoil models or as input parameters for turbulence models in CFD simulations. Therefore, the hot film was also used to quantify the freestream turbulence under both static and dynamic flow conditions. For both cases, turbulence intensity was measured several times at a single midspan coordinate in the test section. In the steady flow case, the choke vane drive motor is operated for the first half of the test duration to enable an in situ calibration of the film. For the remainder of the test, the choke vane drive motor was turned off. In the dynamic case, turbulence statistics are extracted from hot-film data acquired for 1 Hz $< f_{\mathrm{CV}} <$ 10 Hz via the procedure outlined earlier. The intensity of high-frequency velocity fluctuations is juxtaposed by applying a digital bandpass filter (100 Hz < passband < 5 kHz) to steady and unsteady flow velocity signals alike. The lower bound of 100 Hz was sufficient to remove contributions of low-frequency velocity oscillations for all cases. The frequency response of this hot film is estimated to be on the order of 1 kHz; therefore, turbulence intensity estimates are representative of a limited frequency band. For steady flow, the turbulence intensity at the center of the test section is approximately 0.2% of the local freestream velocity for $M \approx 0.44$. When the vanes are rotating at any frequency discussed in this paper, the turbulence intensity of high-frequency velocity fluctuations is doubled to 0.45% of the average freestream velocity for $M_{\mathrm{avg}} \approx 0.52$.

III. Computational Methodology

A. One-Dimensional Analysis

A theoretical analysis was conducted based on 1-D isentropic relations to provide a basic understanding of the oscillating freestream behavior. At a given rotating speed ($\mathrm{d}\theta_{\mathrm{CV}}/\mathrm{d}t$) deduced from the optical encoder signal, the function of throat area with respect to time is derived based on the choke vane geometrical parameters (see inset in Fig. 4). The height of the tunnel at the cross section of the choke vanes is H (66 cm), while d and e are the major (6.5 cm) and minor (4.1 cm) axes of the elliptical vane profile, respectively. The 1-D analysis also includes a first-order correction based on steady mean flow, turbulent boundary-layer displacement thickness for the effective flow area reduction at the test section and throat due to viscous layers on all four walls [22]. For this correction, the boundary-layer initiation location is taken to be the beginning of the straight duct, 0.95 m upstream of the test section.

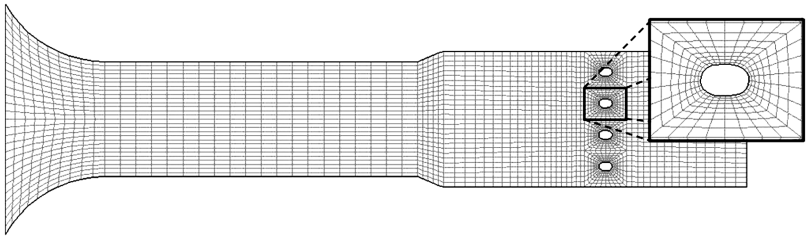

Fig. 7 Computational grid for horizontal vane orientation. The mesh is generated using Gambit.

B. Two-Dimensional Analysis of Oscillating Freestream

Two-dimensional simulations of the unsteady flow scenarios were also conducted using the commercially available ANSYS FLUENT (version 6.3.16) to study the characteristics of the choke vane disturbance as it propagates upstream and to serve as a useful reference for future experiments. Thus, the inviscid flow model is used for unsteady simulations.

Accordingly, a coarse, structured mesh was generated using ANSYS Gambit, and the computation requirements are minimal. Figure 7 displays the computational grid, with the choke vanes in their horizontal orientation. It is noted that the grid used for these simulations imposes a rigid wall boundary everywhere, while in reality, the walls on the top and bottom of the test section are perforated and the plenums are open downstream of the test section in order to minimize reflected shocks off a would-be airfoil in the test section. The actual porosity of the perforated walls is 10%, and the effective porosity has been determined in previous studies [16] to be 6%. Thus, the rigid wall assumption is a suitable approximation.

The direct approach to simulating the unsteady flow conditions is to use an unstructured dynamic mesh. Accordingly, the rotation of the choke vanes can be specified, and the grid can be updated at each time step. However, since the mesh is coarse for the inviscid model, the rotation of the vanes significantly compromises the mesh quality near the vanes, which can cause the solution to diverge. The large amount of computation time required to run the solver with an adequately refined mesh rendered the model impractical for the present circumstances.

The primary motive for modeling this unsteady, compressible flow regime is to predict the upstream propagation speed and attenuation of the choke vane disturbance. The choke vane rotation essentially produces an oscillating back pressure. Therefore, in lieu of employing a dynamic mesh, the inlet total pressure is set to match the experimental conditions, and the unsteady flow is simulated by prescribing a sinusoidal variation of pressure at the throat while the choke vanes remain fixed in the horizontal position. The absolute backpressure function is expressed in kilopascals in Eq. (4). The parameter set

$$\{P_{\text{avg}} = 175.8 \text{ kPa}, B = 10.3 \text{ kPa, and } \varphi \approx -\pi/8 \text{ rad}\}$$

was determined to produce Mach number oscillations that are closest to the experimental data at a Mach number oscillation frequency $f_M = 2.5$ Hz. The solutions are then computed using a second-order implicit scheme and the coupled solver in Fluent for the same parameter set and a range of oscillation frequency:

$$P_{\text{exit}} = P_{\text{avg}} + B\sin(\theta_M - \varphi + \pi) \quad \text{for } 0 < \theta_M < 2\pi \qquad (4)$$

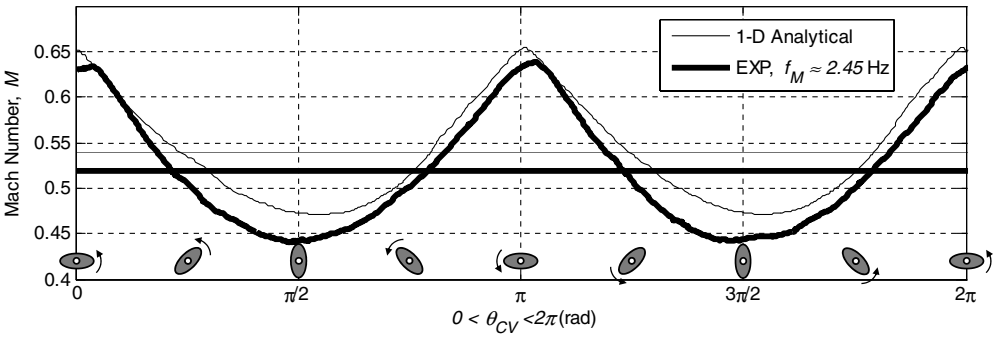

a) Mach number vs choke vane angular position

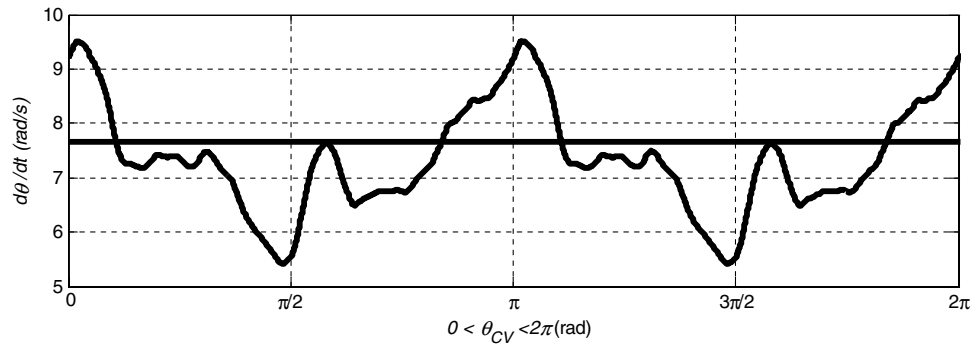

b) Choke vane angular velocity vs angular orientation

Fig. 8 Choke vane angular position vs a) test-section Mach number and b) instantaneous choke vane angular speed. In Fig. 8a, results of 1-D analysis are compared with experimental hot-film data.

IV. Results and Discussion

A. Unsteady Mach Number Oscillations

Mach number data acquired with a hot film are compared with an analytical 1-D approximation in Fig. 8a. The Mach number oscillation frequency f_M is 2.45 Hz, and the experimental waveform data is shifted in phase by $\varphi \approx -\pi/8$ to be aligned with the analytical waveform produced by the choke vane disturbance. The analytical result is obtained using the area-Mach number relation [Eq. (1)] and the physical throat area displayed in the inset of Fig. 4. The time dependency of A^* in Fig. 4 is obtained by using the choke vane angular position θ_{CV} information obtained with the shaft-mounted optical encoder. The corresponding phase-averaged angular velocity of the uppermost rotating choke vane is plotted beneath the Mach number in Fig. 8b.

Since there are two Mach number oscillations for each full choke vane revolution, for $f_M = 2 \times f_{CV} \approx 2.45$ Hz, the average angular velocity ($d\theta_{CV,avg}/dt$) is 7.7 rad/s, although the rate is not constant. Evidently, the choke vane accelerates ($\pi/2 + m\pi < \theta_{CV} < \pi + m\pi$, $d^2\theta_{CV}/dt^2 > 0$) to the orientation of minimum blockage ($\theta_{CV} = m\pi$) and decelerates ($m\pi < \theta_{CV} < \pi/2 + m\pi$, $d^2\theta_{CV}/dt^2 < 0$) toward the orientation of maximum blockage ($\theta_{CV} = \pi/2 + m\pi$). This unsteady rotation speed is due to variation in the moment applied to the choke vanes, which is in turn due to varying aerodynamic loading as a function of vane orientation. If one considers the configuration of the vanes as an alternating set of converging and diverging nozzles (see throat area of Fig. 5), there will be alternating regions of subsonic and supersonic flow within a given cross section of the vanes. The local pressure distribution on the vanes will not be symmetric about the centerline of the vane due to the nonlinear relationship between local Mach number and static pressure. Application of idealized 1-D isentropic theory reveals that the pressure differences lead to a net moment in the same direction as the rotation during vane phase positions ($\pi/2 + m\pi < \theta_{CV} < \pi + m\pi$), while the net moment is against the rotation direction for phase positions ($m\pi < \theta_{CV} < \pi/2 + m\pi$). The time-varying moment results in an unsteady choke vane angular rate of rotation, with less time spent at the minimum blockage area (horizontal). Consequently, the peak of the Mach number oscillation is narrow (minimum blockage), and the valley of the waveform is broadened (maximum blockage). Thus, the Mach number oscillation waveform produced by the implemented choke vane geometry is only approximately sinusoidal. Although the 1-D calculation captures the general shape of the waveform, the hot-film data show that the actual waveform exhibits features similar to a wave breaking. A 1-D approximation of the instantaneous wave speed c is given by Eq. (5), where M is the instantaneous Mach number and a is the local speed of sound, which is approximately constant during the test. Accordingly, as the Mach number decreases, the speed of the wave traveling against the flow direction increases and vice versa, causing the waveform to lean. While measuring unsteady airstream modulation in a similar facility, Babinsky and Fernie [11] also observed this wave-steepening phenomenon to varying degrees, depending on the upstream distance from the throat:

$$c \approx a(1 - M) \tag{5}$$

Regarding extreme values of the waveform, there is a notable discrepancy between the 1-D approximation and the measured Mach number. This discrepancy is more pronounced at the minimum than at the maximum values. The 1-D approximation overpredicts the maximum Mach number by 2.4% while overpredicting the minimum by 6.7%. Furthermore, the mean Mach number from the 1-D analysis is 0.54 (4.2% greater than the measured value) and the oscillation amplitude is 0.18 (7.1% less than the measured value). It is surmised that these differences are due, at least in part, to the fact that the 1-D approximation does not incorporate effective area changes resulting from the dynamic evolution of viscous layers throughout the tunnel.

Representative test-section Mach number oscillations from an experiment where the vane oscillation frequency was varied slowly and continuously throughout the course of a 60 s interval are presented in Fig. 9. The waveforms are plotted against the Mach number oscillation period for four different forcing frequencies. The optical encoder, which is coupled to a choke vane shaft, was used to reconstruct the Mach number waveform at the throat. The phase of the test-section Mach number oscillation with respect to the throat is determined by evaluating the temporal correlation between the Mach number waveform measured at the test section and the Mach number waveform reconstructed at the throat location.

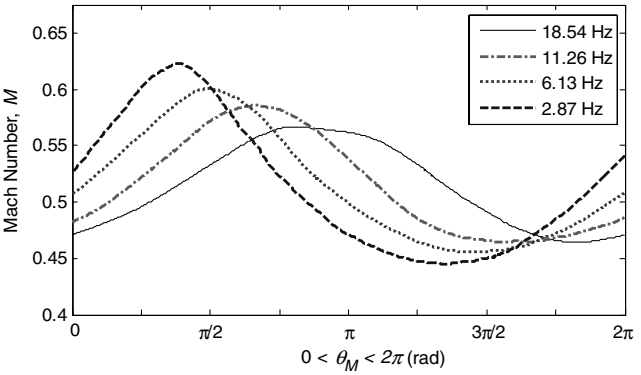

Fig. 9 Representative measured Mach number oscillations at different forcing frequencies.

As discussed regarding Fig. 8, the waveform produced by the fabricated choke vane geometry is inherently peaky at the high Mach number while the valleys of the oscillation are protracted. This is especially evident at the low oscillation frequencies (e.g., $f_M \approx 2.9$ Hz, maximum $\theta_M = \pi/3$, and minimum $\theta_M = 4\pi/3$ in Fig. 9). As f_M is increased and higher frequency content is attenuated, the peak is smeared and the waveform better resembles the shape of a true sinusoid.

In addition to the pronounced decrease in amplitude shown for a range of forcing frequencies in Fig. 9, as f_M increases, there is a significant phase shift between the choke vane orientation and the test-section Mach number. Thus, the flow exhibits features of a low-pass filter. This quality may be essential to achieving a variety of amplitude and phase conditions.

B. Dynamic Mach Number Oscillation Characterization

Experimental and computational studies were conducted to evaluate the dynamic freestream characteristics with respect to Mach number oscillation frequency. Figure 10 includes Bode plots showing the normalized amplitude (Fig. 10a) and the phase relationships versus forcing frequency f_M (Fig. 10b). In addition, Fig. 10c displays the mean Mach number behavior as a function of Mach number oscillation frequency. The amplitude results are normalized by the amplitude measured at a Mach number oscillation frequency of 2.5 Hz. Therefore, the monotonically decreasing slope of the amplitude function indicates that the amplitude is reduced with respect to the 2.5 Hz case, as seen previously in Fig. 9. The predictive value of the computational model is validated over the range of frequencies tested. Both the experimental and computational results indicate that the amplitude is reduced by approximately 3 dB for a roll-off frequency of $f_M \approx 8$ Hz.

In Fig. 10a, for 7 Hz $< f_M <$ 9 Hz and 13 Hz $< f_M <$ 17 Hz, the roll-off characteristic exhibits a notable deviation from an otherwise logarithmic decay. This discontinuity is presumed to correspond to an acoustic resonance in the wind tunnel. In accord with this assumption, an analytical solution for the natural frequency f_m of a cavity connected to a transmitting tube is cited from [21]. Evaluating the analytical solution in Eq. (6), using the dimensions shown in Fig. 1, provides a first-order approximation in an attempt to corroborate this assumption. The characteristic length ($L = 3.5$ m) is chosen to be the upstream distance from the throat to the last screen in the stagnation chamber. The radius ($r = 0.6$ m) and the volume ($V = 3.5$ m^3) are dimensions of the stagnation chamber. The relevant wave speed c_{avg} is discussed in depth in Sec. IV.C. The first

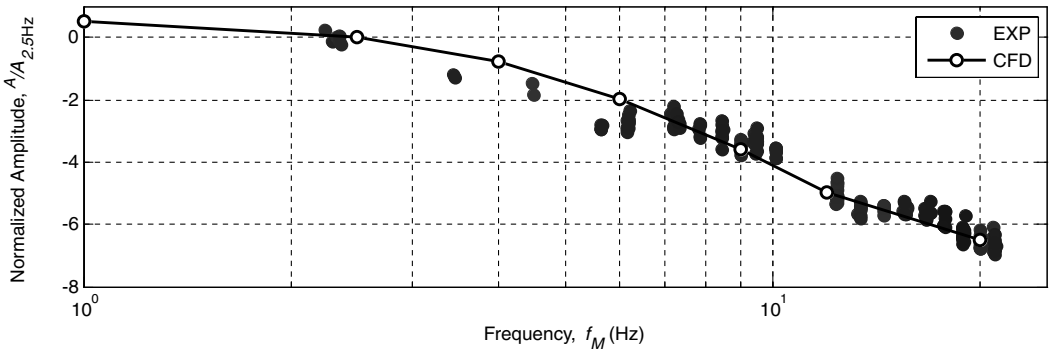

a) Gain

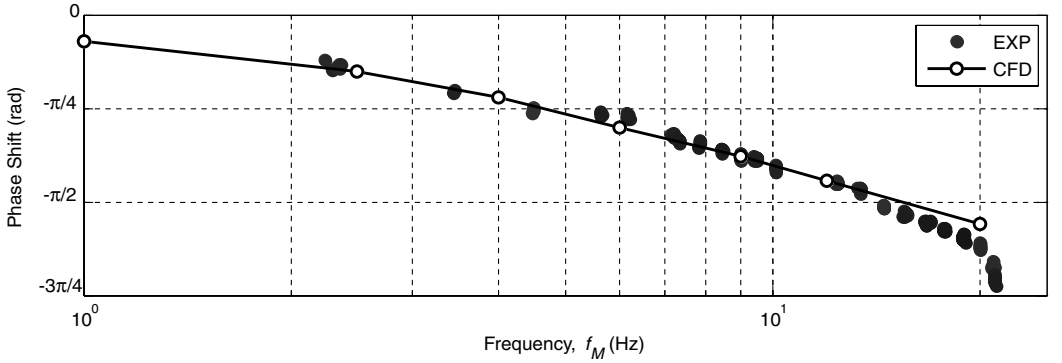

b) Phase

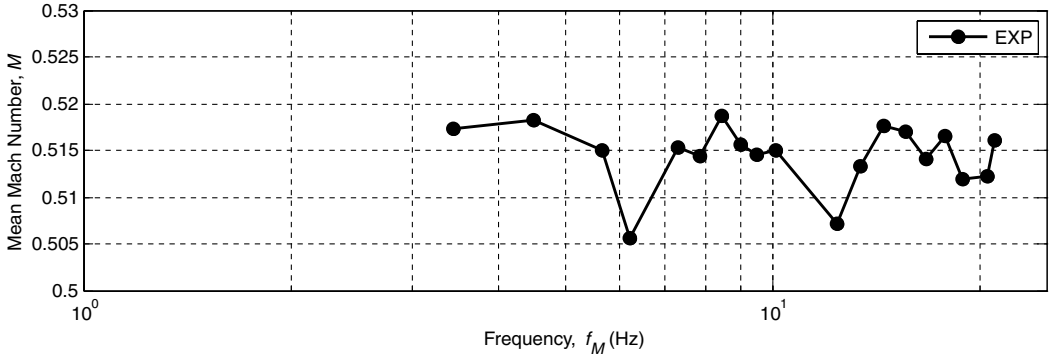

c) Mean Mach number

Fig. 10 Mach number oscillation frequency f_M vs a) amplitude, b) phase and, c) mean Mach number.

and second harmonic frequencies obtained by evaluating this expression are approximately 6.5 and 13 Hz:

$$f_m = \sqrt{\frac{3\pi m^2 r^2 c_{\text{avg}}^2}{4LV}} \tag{6}$$

Figure 10b shows the phase shift of the test-section Mach number waveform with respect to the throat. As with the oscillation amplitude predictions, the phase predictions are validated through the range of oscillation frequencies tested. The most noteworthy feature in this figure is that the phase shift is linear with frequency, which suggests that the wave speed does not vary appreciably with frequency. For an oscillation frequency increment of 1 Hz, the approximate shift in phase is $-\pi/36$ rad.

Figure 10c displays the mean Mach number as a function of Mach number oscillation frequency along the same scale as the Bode plots to easily show that features of this curve are coincident with the aforementioned features exhibited in the gain Bode plot. Over the range of frequencies tested, the overall average mean Mach number is approximately 0.515. At $f_M \approx 6.2$ Hz and 12.4 Hz, the mean Mach number is reduced by approximately 2% compared with the overall average. This coincides with the acoustic resonance frequencies calculated using Eq. (6).

C. Disturbance Propagation Characterization

An initial concern in the design of this tunnel modification was the convection speed of the downstream disturbance to the test section for communicating changes in Mach number. Figure 11 summarizes the average speed c_{avg} at which the choke vane disturbance propagates upstream along the centerline of the wind tunnel. This plot was produced by performing temporal correlations between pressure data recorded at any two static pressure taps along the constant area duct (Fig. 5, taps 2–5), as outlined in Sec. II.C. The test-section tap (tap 3; $x = 0$ m) was arbitrarily chosen to be the reference location. The distance of each tap from the test section is plotted along the ordinate. The time shift required to align the various pressure signals with that of the test section is plotted along the abscissa. Since the duct is of constant area (6×22 in.), a linear fit is appropriately applied to the

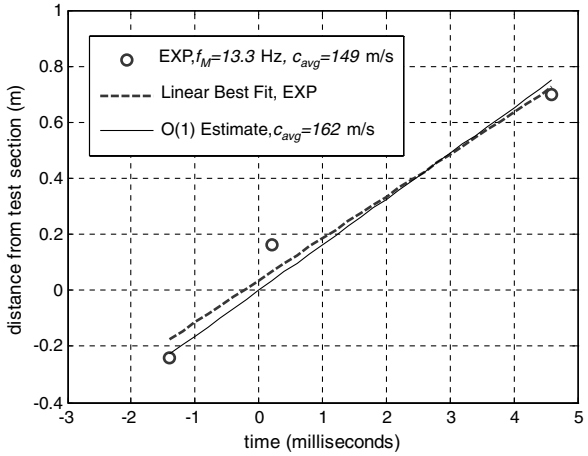

Fig. 11 Measured and predicted wave speed for $f_M = 13.3$ Hz. The average wave speed c_{avg} is estimated by the slope of a linear fit and tabulated in the legend. First-order estimate is predicted with Eq. (5) $\{M_{\text{avg}} = 0.515, T_f = 280$ K$\}$.

data for each case, and the slope is the approximate wave speed throughout the test section. The average wave speed is tabulated in the legend for each case.

Figure 11 shows experimental data for a forcing frequency of 13.3 Hz along with a 1-D approximation given by Eq. (5). The experimental and estimated values of the wave speed c_{avg} for $M_{\text{avg}} = 0.515$ and $T_f = 280$ K are 149 and 162 m/s, respectively (a difference of 8%). Thus, Eq. (5) is a valid approximation for the wave speed. Furthermore, the wave speed can be estimated for a range of frequencies using the data in Fig. 10c. The experimental value of the convective speed indicates that the propagation time for a wave traveling from the throat to the test section will be approximately 11.4 ms.

V. Conclusions

The 6×22 in. transonic wind tunnel at OSU was modified to produce an approximately sinusoidal Mach number oscillation ($0.44 < M < 0.65$) at a frequency f_M up to 25 Hz by dynamically varying the choking area downstream of the test section. An investigation was conducted using 1-D analytical theory, 2-D CFD simulation, and experimental measurement to characterize the device developed to oscillate the wind-tunnel airstream. A critical aspect of the experimental investigation included the development of an in situ hot-film calibration procedure, which was dictated by a variety of instrumentation and facility limitations. The measured Mach number waveform is not a pure sinusoid, owing to unsteady choke vane rotation speed, which is explained by the time-varying aerodynamic moments about the vane axis of rotation.

The amplitude and phase shift of Mach number oscillation were characterized for varying oscillation frequency. Oscillation amplitude is attenuated significantly at high oscillation frequencies. Bode plots indicate that the -3 dB roll-off point is approximately 8 Hz. Resonant modes in the wind tunnel were observed at oscillation frequencies of 6.5 and 13 Hz and are explained by 1-D acoustic theory. In conjunction with the experimental investigation, an inviscid computational model of the wind-tunnel facility was validated along the centerline of the wind tunnel over a range of oscillation frequencies. The model correctly predicts both the magnitude attenuation and phase shift behavior of the Mach number oscillations produced. Finally, the upstream propagation speed of the wave produced by the choke vane disturbance was measured to be 149 m/s at $f_M \approx 13.3$ Hz. A first-order approximation of the propagation speed is within 8% of the measured value, providing a suitable estimate for design of experiment.

The transonic wind tunnel has been modified, and predictive tools have been assembled to prepare for a wide range of unsteady compressible flow applications. For example, modifications can be made to enable the evaluation of various flow control applications or of dynamic stall and gust simulation. Various diagnostic techniques, including particle image velocimetry and pressure sensitive paint, are also being developed for use in this facility.

Acknowledgments

The authors thank John D. Lee, Jolanta Janiszewska, and Mary Berchak for fruitful discussions about the original design, construction, and operation of the 6×22 in. transonic wind tunnel.

References

[1] Goodrich, M., and Gorham, J., "Wind Tunnels of the Western Hemisphere," Federal Research Division Library of Congress, Washington, D.C., 2008.

[2] Retelle, J. P., McMichael, J. M., and Kennedy, D. A., "Harmonic Optimization of a Periodic Flow Wind Tunnel," *Journal of Aircraft*, Vol. 18, No. 8, 1981, pp. 618–623. doi:10.2514/3.44727

[3] Pierce, G. A., Kunz, D. L., and Malone, J. B., "The Effect of Varying Freestream Velocity on Airfoil Dynamic Stall Characteristics," *Journal of the American Helicopter Society*, Vol. 23, No. 2, 1978, pp. 27–33. doi:10.4050/JAHS.23.27

[4] Favier, D., Agnes, A., Barbi, C., and Maresca, C., "Combined Translation/Pitch Motion: A New Airfoil Dynamic Stall Simulation," *Journal of Aircraft*, Vol. 25, No. 9, 1988, pp. 805–814. doi:10.2514/3.45663

[5] Favier, D., Maresca, C., and Rebont, J., "Dynamic Stall Due to Fluctuations of Velocity and Incidence," *AIAA Journal*, Vol. 20, No. 7, 1982, pp. 865–871. doi:10.2514/3.51145

[6] Favier, D., Rebont, J., and Maresca, C., "Large-Amplitude Fluctuations of Velocity and Incidence on an Oscillating Airfoil," *AIAA Journal*, Vol. 17, No. 11, 1979, pp. 1265–1267. doi:10.2514/3.7622

[7] Maresca, C., Favier, D., and Rebont, J., "Unsteady Aerodynamics of an Aerofoil at High Angle of Incidence Performing Various Linear Oscillations in a Uniform Stream," *Journal of the American Helicopter Society*, Vol. 26, No. 2, 1981, pp. 40–45. doi:10.4050/JAHS.26.40

[8] Ham, N. D., Bauer, P. H., and Lawrence, T. L., "Wind Tunnel Generation of Sinusoidal Lateral and Longitudinal Gusts by Circulation Control of Twin Parallel Airfoils," NASA CR 137547, 1974.

[9] Szumowski, A. P., and Meier, G. E. A., "Forced Oscillations of Airfoil Flows," *Experiments in Fluids*, Vol. 21, No. 6, 1996, pp. 457–464. doi:10.1007/BF00189048

[10] Selerowicz, W. C., and Szumowski, A. P., "Airfoil Flow Instabilities Induced by Background Flow Oscillations," *Experiments in Fluids*, Vol. 32, 2002, pp. 441–446. doi:10.1007/s00348-001-0377-4

[11] Babinsky, H., and Fernie, R. M., "NACA0012 Aerofoil in an Oscillating Freestream," 40th AIAA Aerospace Sciences Meeting and Exhibit, Reno, NV, AIAA Paper 2002-0115, 2002.

[12] Fernie, R. M., and Babinsky, H., "Unsteady Shock Behaviour on a NACA0012 Aerofoil," 41st AIAA Aerospace Sciences Meeting and Exhibit, Reno, NV, AIAA Paper 2003-0226, 2003.

[13] Fernie, R. M., and Babinsky, H., "Unsteady Shock Motion on a NACA0012 Aerofoil at Low Reduced Frequencies," 42nd AIAA Aerospace Sciences Meeting and Exhibit, Reno, NV, AIAA 2004-0049, 2004.

[14] Fernie, R. M., "Low Frequency Shock Motion on a NACA 0012 Aerofoil," Ph.D., Dissertation, Kings College, Univ. of Cambridge, Cambridge, England, U.K., Oct. 2004.

[15] Bruce, P. J. K., and Babinsky, H., "Unsteady Shock Wave Dynamics," *Journal of Fluid Mechanics*, Vol. 603, 2008, pp. 463–473. doi:10.1017/S0022112008001195

[16] Lee, J. D., Gregorek, G. M., and Korkan, K. D., "Testing Techniques and Interference Evaluation in the OSU Transonic Airfoil Facility," 11th Fluid and Plasma Dynamics Conference, Seattle, WA, AIAA Paper 1978-1118, 1978.

[17] Gregorek, G. M., Hoffman, M. J., and Berchak, M. J., "Steady State and Oscillatory Aerodynamic Characteristics of a NACA 0015 Airfoil," Ohio State Univ., Aeronautical and Astronautical Research Lab. Data Report, Columbus, OH, 1989.

[18] Petrie, S. L., and Davis, J. A., "Unsteady Transonic Aerodynamics," Columbus, OH, *Symposium on Airfoils and Aviation, Proceedings of the Annual Conference for Engineers*, May 1978.

[19] Coleman, H. W., and Steele, W. G., *Experimentation and Uncertainty Analysis for Engineers*, 2nd ed., Wiley-Interscience, New York, 1999, pp. 94–98.
[20] Collis, D. C., and Williams, M. J., "Two-Dimensional Convection from Heated Wires at Low Reynolds Number," *Journal of Fluid Mechanics*, Vol. 6, No. 3, 1959, pp. 357–384. doi:10.1017/S0022112059000696
[21] Wheeler, A. J., and Ganji, A. R., *Introduction to Engineering Experimentation*, Prentice–Hall, Upper Saddle River, NJ, 1996, pp. 154–189, 343–357.
[22] White, F. M., *Viscous Fluid Flow*, McGraw–Hill, New York, 1991, p. 220.

L. Cattafesta
Associate Editor